Urban Water Journal

ISSN: (Print) (Online) Journal homepage: https://www.tandfonline.com/loi/nurw20

Sediment transport prediction in sewer pipes during flushing operation

Carlos Montes, Hachly Ortiz, Sergio Vanegas, Zoran Kapelan, Luigi Berardi & Juan Saldarriaga

To cite this article: Carlos Montes, Hachly Ortiz, Sergio Vanegas, Zoran Kapelan, Luigi Berardi & Juan Saldarriaga (2022) Sediment transport prediction in sewer pipes during flushing operation, Urban Water Journal, 19:1, 1-14, DOI: 10.1080/1573062X.2021.1948077

To link to this article: https://doi.org/10.1080/1573062X.2021.1948077

URBAN WATER JOURNAL
2022, VOL. 19, NO. 1, 1–14
https://doi.org/10.1080/1573062X.2021.1948077

Taylor & Francis
Taylor & Francis Group

RESEARCH ARTICLE

Sediment transport prediction in sewer pipes during flushing operation

Carlos Montes [a], Hachly Ortiz [a], Sergio Vanegas [a], Zoran Kapelan [b], Luigi Berardi [c] and Juan Saldarriaga [a]

[a]Department of Civil and Environmental Engineering, Universidad de los Andes, Bogotá, Colombia; [b]Department of Water Management, Delft University of Technology, Delft, Netherlands; [c]Department of Engineering and Geology, Università Degli Studi "G. d'Annunzio" Chieti, Pescara, Italy

ABSTRACT

This paper presents a novel model for predicting the sediment transport rate during flushing operation in sewers. The model was developed using the Evolutionary Polynomial Regression Multi-Objective Genetic Algorithm (EPR-MOGA) methodology applied to new experimental data collected. Using the new model, a series of design charts were developed to predict the sediment transport rate and the required flushing operation time for several pipe diameters. Accurate results (i.e. sediment transport rates) were obtained when applied to a case study in a combined sewer pipe in Marseille, as reported in the literature. The novelty of the model is the inclusion of the pipe slope, the inflow 'dam break' hydrograph, and the sediment properties as explanatory parameters. The new model can be used to predict flushing efficiency and design new flushing cleaning schedules in sewer systems.

ARTICLE HISTORY
Received 19 February 2021
Accepted 21 June 2021

KEYWORDS
Flushing efficiency; sediment transport; sewer cleansing; sewer flushing

1. Introduction

Sediment deposition and accumulation are well-known issues in sewer systems modelling. The presence of permanent deposits of material at the bottom of sewer pipes produces several problems, such as reduced flow capacity and premature combined sewer overflows (Ashley et al. 2004; Rodríguez et al. 2012). Flushing waves, also known as surge flushing technique, have been identified as an efficient (Bong, Lau, and Ab Ghani 2016; Yang et al. 2019) and cost-effective (Campisano et al. 2019; Campisano, Creaco, and Modica 2007) method for solving these problems. It aims to remove the deposited sediments by generating waves, which are produced by the upstream storage and further discharge of water volumes. These flushing waves increase the bottom shear stress and induce the scour and resuspension of the deposited material.

The above flushing technique has been applied in several case studies following operational and management practice guides (Fan 2004; Saegrov 2006; NEIWPCC 2003) in countries such as Germany, France, the USA and the UK. As an example, Saegrov (2006) suggest flushing waves to remove settled deposits in sewers ranging from 100 mm to 1200 mm pipe diameter with a mandatory cleaning frequency once in 1 to 5 years. However, these guides do not specify important flushing parameters such as the hydraulic and pipe characteristics (i.e. length, slope and hydraulic roughness, among others), sediment properties and flushing volume. The lack of information on these specifications has contributed to the fact that existing flushing practices tend to be oversized. As an instance, Dettmar (2007) compared design tables developed by using extensive field studies and mathematical simulations (Chebbo et al. 1996; Dettmar 2005; Lainé et al. 1998) and concluded that smaller flushing volumes and water storage heights achieve the same flushing length and efficiency in removing the volume of deposited sediments, compared to operational and management practice guides.

In the last decades, several studies have quantified the flushing efficiency in terms of (a) reduction of volume and/or weight of sediments (Bong, Lau, and Ab Ghani 2016; Campisano et al. 2019; Campisano, Creaco, and Modica 2008, 2004; Creaco and Bertrand-Krajewski 2009; Guo et al. 2004; Ristenpart 1998; Shahsavari, Arnaud-Fassetta, and Campisano 2017), (b) changes in deposited bed thickness (Bong, Lau, and Ab Ghani 2013, 2016; Campisano et al. 2019; Campisano, Creaco, and Modica 2008, 2007, 2004; Dettmar, Rietsch, and Lorenz 2002; Ristenpart 1998; Shahsavari, Arnaud-Fassetta, and Campisano 2017; Shirazi et al. 2014), (c) variation of concentrations of total suspended solids (Ristenpart 1998; Sakakibara 1996), (d) increase in the bottom shear stress (Bertrand-Krajewski et al. 2003; Campisano, Creaco, and Modica 2008; Campisano and Modica 2003; Dettmar, Rietsch, and Lorenz 2002; Ristenpart 1998; Schaffner and Steinhardt 2006; Yang et al. 2019), (e) length of the channel that can be potentially cleaned (Bertrand-Krajewski et al. 2003; Bong, Lau, and Ab Ghani 2013; Dettmar, Rietsch, and Lorenz 2002; Shahsavari, Arnaud-Fassetta, and Campisano 2017; Yang et al. 2019) and (f) stored water volume discharged (Bertrand-Krajewski et al. 2003; Dettmar, Rietsch, and Lorenz 2002; Fan et al. 2001). These studies were carried out in both laboratory and real sewer flumes using different sediment characteristics, stored water volumes and geometrical characteristics of the flume. As a result, a list of parameters affecting the flushing efficiency was identified and classified in three main groups: (i) flushing hydraulics, (ii) pipe geometry and (iii) sediment properties. Flushing hydraulic parameters include water velocity (V_f), shear stress (τ), the water level in the pipe (Y), flowrate (Q), stored water head (h_o) and stored water volume discharged (V_a). In the pipe

CONTACT Carlos Montes cd.montes1256@uniandes.edu.co

geometry, parameters as the slope (S_o), diameter (D), length (L), cross-section shape factor (β) and composite roughness (k_c) have been included. Finally, sediment properties include mean particle diameter (d), sediment thickness (y_s) and width (W_b), specific gravity (SG), porosity (η) and density (ρ_s).

The previous three groups of parameters have been used for implementing numerical models useful to quantify the flushing efficiency. Models found in the literature are focused on (i) solving complex mathematical structures, (ii) proposing simple dimensionless equations for estimating sediment transport rates and (iii) using Machine Learning (ML) and Artificial Intelligence (AI) techniques for finding patterns in data and predicting bedload and suspended load transport.

In the first approach, the one-dimensional Saint-Venant equations (Campisano, Creaco, and Modica 2006; Campisano and Modica 2003; De Sutter, Huygens, and Verhoeven 1999), coupled with the Exner equation for uniform (Campisano, Creaco, and Modica 2007, 2004; Creaco and Bertrand-Krajewski 2009; Shirazi et al. 2014) and non-uniform (Campisano et al. 2019) sediments, are used for predicting bed sediment thickness changes during the flushing operation. More complex models involve the two-dimensional (Caviedes-Voullième et al. 2017; Yu and Duan 2014) and three-dimensional (Schaffner and Steinhardt 2006) solutions of the Saint-Venant equations. An example of the literature models is as follows:

$$\frac{\partial U}{\partial t} + \frac{\partial F(U)}{\partial x} = D(U) \tag{1}$$

where U, $F(U)$ and $D(U)$ are defined as follows:

$$U = \begin{bmatrix} A \\ Q \\ A_s \end{bmatrix}; F(U) = \begin{bmatrix} Q \\ V_f Q + \frac{F_h}{\rho} \\ \frac{1}{1-\rho} Q_s \end{bmatrix}; D(U) = \begin{bmatrix} 0 \\ gA\left(S_o - \frac{{V_f}^2}{{k_c}^2 R^{4/3}}\right) \\ 0 \end{bmatrix} \tag{2}$$

where F_h is the hydrostatic force over the cross-section, ρ the water density, R the hydraulic radius, A is the cross-section wetted area, A_s is the cross-section sediment bed area and Q_s the sediment flow rate.

In the second approach mentioned above, several authors have developed analytical equations for predicting the number of flushes required to move the deposited sediment bed (Bong, Lau, and Ab Ghani 2013; Chebbo et al. 1996). Likewise, the effects of pipe slope, bottom roughness, storage water level, and downstream water level, among others (Yang et al. 2019; Kuriqui, Koçileri, and Ardiçlioğlu 2020) have also been studied in the past. As an example, Bong, Lau, and Ab Ghani (2013) proposed the following equation, where n_f is the number of flushes required to move the deposited sediment bed by 1 m:

$$n_f = 251.43 y_s + 6.57 \tag{3}$$

In the third approach, several studies using ML and AI have been developed for predicting both bedload and suspended load transport in sewers, flumes, and streams. Several techniques as Artificial Neural Networks (Wan Mohtar et al. 2018; Bajirao et al. 2021), Random Forests (Khosravi et al. 2020; Safari 2020; Montes, Kapelan, and Saldarriaga 2021), and Vector Machines (Ebtehaj et al. 2017), among others, have been trained with experimental data collected at laboratory scale and tested with benchmark data found in the literature. These models outperform traditional regression formulas during the training stage but tend to underperform when applied to external datasets collected in sewers and flumes (Montes, Kapelan, and Saldarriaga 2021), i.e., during the testing stage.

Numerical studies mentioned above, based on the solution of the Saint-Venant and Exner coupled-equations for sediment transport under unsteady flow conditions, show similar predictions of the sediment thickness changes compared to the experimental data collected, i.e., the models show good accuracy prediction. Despite the solutions and simulations based on Saint Venant-Exner equations showing good accuracy, in practice, the application for operational and management practices is complex and non-pragmatic. Also, the analytical and dimensionless equations proposed by Bong, Lau, and Ab Ghani (2013) and Yang et al. (2019), do not include important parameters such as the pipe/flume geometry and the sediment characteristics. Finally, AI and ML models are largely black-box models (Montes, Kapelan, and Saldarriaga 2021), limiting their interpretability for practical applications.

The above gaps are addressed here by developing a new parsimonious regression-based model using the Evolutionary Polynomial Regression – Multi-Objective Genetic Algorithm (EPR-MOGA) (Giustolisi and Savic 2009) strategy. EPR-MOGA is a data-driven method which combines genetic algorithm with evolutionary computing for finding polynomial structures. Due to its characteristics, the returned symbolic expressions can be compared with existing models in terms of the input variables, exponent coefficients, and technical insight on the phenomenon (Montes et al. 2020a) while reducing the risk of overfitting.

This paper aims to propose a new model for predicting the sediment transport rate during flushing operations in sewers. The novelty of this model is the inclusion of flushing 'dam break' hydrograph, pipe geometry, and deposited sediment characteristics in a simple polynomial expression. The new model developed here can be used to optimize flushing schemes and reduce the volume of water required for cleaning sewers.

2. Experimental methods and data collection

The collection of experimental data was carried out in two pipes with diameters of 209 mm and 595 mm (Montes et al. 2020b), both located at the Hydraulics Laboratory of the University of the Andes, Colombia. A sediment bed with a near-uniform thickness and width was prepared at the bottom of the pipes, using uniformly graded sediment material ranging from 0.21 mm to 2.6 mm. These particles had a specific gravity between 2.57 and 2.67, which was calculated using the pycnometer method (ASTM D854-14 2014). The experiments were carried out under unsteady flow conditions, simulating the 'dam break' waves produced during a flushing event. The methodology used for data collection and further details of both experimental setups are described below.

2.1. 209 mm pipe setup

The 209 mm diameter acrylic pipe had a length of 10.58 m and was supported on six hydraulic jacks, which allowed to vary the pipe slope between 0.64% and 1.20%. This pipe was connected

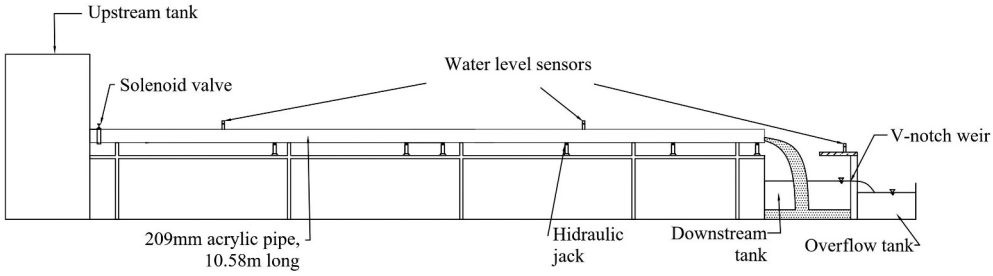

Figure 1. Experimental setup used to collect the unsteady flow data in the 209 mm acrylic pipe.

to a 200 mm solenoid valve, which controlled the inflow into the setup from a 3.5 m^3 upstream tank. A downstream tank with a V-Notch weir was used to measure the water discharge. A real-time water level sensor was used to measure the water height over the weir to calculate the water discharge rate using the V-Notch equation. The calculated discharge was also checked using an ABB- Electromagnetic flowmeter sensor installed upstream of the pipe. Two additional real-time water level sensors were installed along the pipe, aiming to measure the stage hydrograph produced by the flushing waves. Figure 1 shows the general scheme of the experimental setup.

The experimental data was collected as follows. Firstly, the solenoid valve was fully opened, allowing a base flowrate ranging from 0.002 l s^{-1} to 0.414 l s^{-1}. The opening of this valve simulates the 'dam break hydrograph' produced during a flushing operation in a real sewer pipe (e.g. using a Hydrass or a Hydroself flushing gate). Secondly, a sediment bed with near-uniform thickness and width was located at the bottom of the pipe. At this point, the base flowrate helped the formation of the deposited bed along a 3.3 m section. Thirdly, the solenoid valve was completely closed for storing a volume of water between 0.10 m^3 and 0.31 m^3 in the upstream tank. Fourthly, the solenoid valve was opened between 60% and 100% and the opening time was set to 15 sec for all tests. When the first discharged wave reached the sediment bed, the movement of the bed was tracked over time. The sediment velocity (V_s) was calculated using the values of the time and deposited bed displacement during the peak flow. The above procedure was repeated for different accumulated upstream water volume and percentage of the solenoid valve opening.

2.2. 595 mm pipe setup

The pipe was 10.5 m long and supported on a mechanical steel truss, which allowed to modify the slope in a range between 0.04% and 3.44%. The base flow for the experiments, ranging from 1.03 l s^{-1} to 9.98 l s^{-1}, was provided by a 40 BHP pump that supplied water to a 30 m^3 upstream storage which was directly connected to the pipe. For evaluating unsteady flow conditions in this pipe, a second 10 BHP submersible pump was located inside the downstream tank. This pump was directly connected to the upstream tank and was controlled with a variable frequency drive programmed before the experiment to create a pulse with a maximum peak flow of 30 l s^{-1}. Three water level sensors were used to record water depths in the experimental setup. Two of them were installed in the pipe to collect the stage hydrograph, and one was installed in the upstream tank. Full details of the experimental setup were described in Montes et al. (2020b) and are shown in Figure 2.

For this setup, the data was collected as follows. Firstly, the pipe slope was adjusted using the mechanical steel truss and measured with a dumpy level. Secondly, the flow control valve on the upstream tank was opened to supply a base flow to the pipe. Thirdly, a deposited sediment bed with a near-uniform width was prepared at the bottom of the pipe over a minimum length of 1.5 m. At this point, to compare the flushing efficiency under similar conditions, the maximum sediment bed velocity was verified as 0.03 m s^{-1}. If this condition was not fulfilled, the pipe slope or the base flow were changed. Fourthly, the submersible pump, with its variable frequency drive, was activated to simulate the 'dam break hydrograph', which is similar to those produced by the flushing gates in real sewers. The water levels were recorded each 0.025 s and the position of the sediment bed

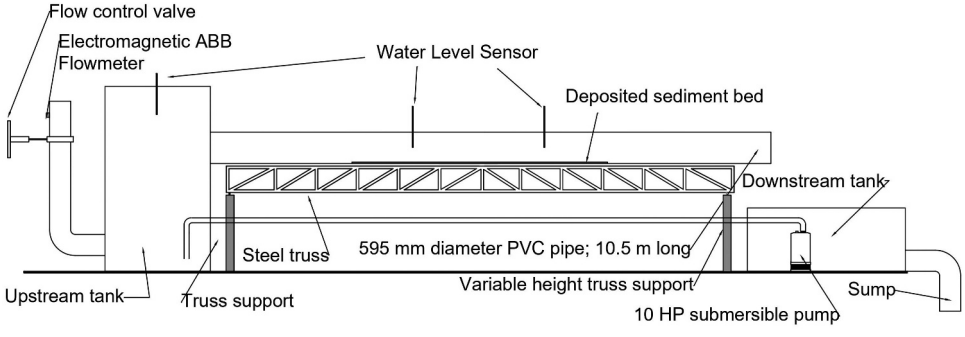

Figure 2. Experimental setup used to collect the unsteady flow data in the 595 mm PVC pipe.

was tracked. The sediment velocity was calculated using the same procedure followed on the acrylic setup.

2.3. Experimental data collected

Using the experimental rig and approach described above, a total of 57 and 64 experiments were carried out in the 209 mm acrylic pipe and 595 mm PVC pipe, respectively. Several variables related to the pipe geometry, sediment properties, and flushing hydraulics, including the base time (t_b), peak time (t_p), base flow (Q_b), and peak flow (Q_p) were recorded in each experiment, as shown in Figure 3. The experimental data collected in both acrylic and PVC pipes are presented in Table 1, where S_o is the pipe slope, D the pipe diameter, Y the water level in the pipe, R the hydraulic radius, d the mean particle diameter, SG the specific gravity, y_s the sediment thickness, V_f the water velocity, and V_s the sediment velocity.

A flushing discharge hydrograph and a plot showing the sediment bed position related with each run are presented in Table 1. The shape and magnitude of the hydrograph are directly related to the sediment bed velocity, and consequently, the sediment bed position. As an example, for six runs, the variation in the sediment bed position and hydrograph characteristics, in both acrylic and PVC pipe, are presented in Figure 4. Full details of each run shown in Figure 4 are presented in Table 1.

Figure 4(a, b) show the relation between the flushing discharge hydrograph and the sediment bed position for tests conducted on the acrylic pipe. As seen in these figures, particle size is a more important variable in defining the sediment position, compared to the peak flow in the hydrograph. Even though the run 82 considers a higher peak flow (Q_p = 5.55 l s^{-1}), the final position of the sediment bed (= 0.41 m) is lower than the run 96 (= 2.62 m) when the peak flow is lower (Q_p = 2.08 l s^{-1}). This occurs because the particle diameter is more relevant compared to the peak flow.

Figure 4(c, d) show the relation between the flushing discharge hydrograph and the sediment bed position for tests in 595 mm setup. The relationship between the discharge hydrograph and the sediment bed position is proportional. For run no. 36 and 61, the mean particle diameter was 2.60 mm, but the pipe slope was 1.65% and 1.82%, respectively. Figure 4(d) shows that maintaining the mean particle diameter constant as the pipe slope increases, the final bed position increases.

3. Model development

3.1. Graphical analysis

A graphical analysis was developed to visualize the relationships between the variables collected in each experiment. The relationship between sediment velocity and flow velocity (V_s/V_f) was plotted against other dimensionless parameters, as shown in Figure 5. These dimensionless parameters have been previously identified as relevant for predicting sediment transport in sewer pipes in previous literature (Ab Ghani and Azamathulla 2011; Ebtehaj and Bonakdari 2016; May et al. 1996; Kuriqui, Koçileri, and Ardiçlioğlu 2020; Montes, Kapelan, and Saldarriaga 2021). Two of these parameters include the dimensionless grain size (d/R) and the Shields parameter (ψ), defined in Equation (4):

$$\psi = \frac{RS_o}{(SG-1)d} \tag{4}$$

Based on the results shown in Figure 5, the following observations can be made:

- In general, higher values of the Shields parameter lead to higher values of V_s/V_f. This can be clearly seen in the acrylic pipe (Figure 5(a)) because of the constant slope value adopted in the experimental rig. Furthermore, high values of S_o and R lead to higher sediment velocities due to higher critical shearing stress (i.e. the applied forces are higher than the submerged weight of the particle). In contrast, deposited materials with high density of particle diameters result in lower sediment velocities.
- The direct relationship between V_s/V_f and the Shields parameter coincides with the inversely proportional relationship between V_s/V_f and d/R, shown in Figure 5(c,d). This is observed because the Shields parameter includes the ratio R/d, as shown in Equation (4).

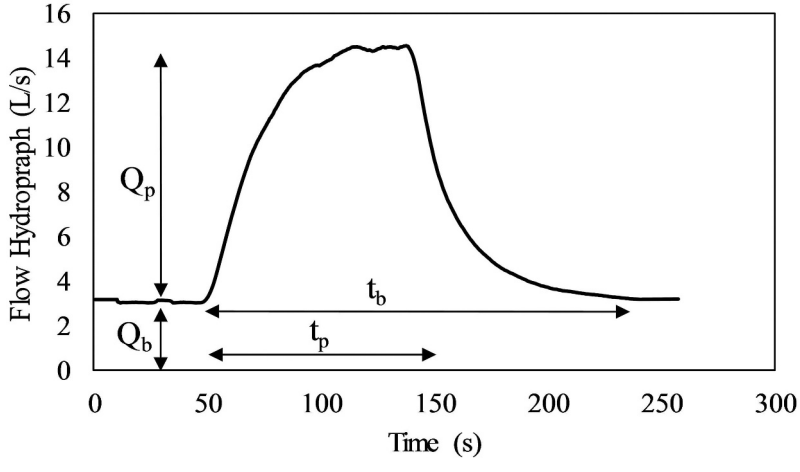

Figure 3. Variable definition of the flushing discharge hydrograph.

Table 1. Experimental data collected for studying flushing waves efficiency on sewer pipes.

Run no.	S_o (%)	D (mm)	Y (mm)	R (mm)	d (mm)	SG (-)	y_s (mm)	t_b (s)	t_p (s)	Q_b (l s^{-1})	Q_p (l s^{-1})	V_f (m s^{-1})	V_s (m s^{-1})
1	0.805	595	70.35	41.96	0.47	2.66	10.14	154	59	5.27	25.48	1.02	0.07
2	0.805	595	57.43	34.62	0.47	2.66	8.26	141	57	5.45	16.76	0.89	0.05
3	0.805	595	53.61	31.34	0.47	2.66	10.53	131	57	5.45	16.49	0.82	0.04
4	1.186	595	57.82	36.46	0.47	2.66	2.49	121	59	4.89	20.53	1.20	0.05
5	1.229	595	54.70	31.17	0.47	2.66	12.55	115	55	4.81	15.97	0.99	0.03
6	1.229	595	61.66	36.67	0.47	2.66	9.91	120	55	5.07	20.27	1.14	0.04
7	1.229	595	50.94	31.92	0.47	2.66	3.90	183	58	1.03	11.10	1.09	0.05
8	1.229	595	67.63	39.54	0.47	2.66	12.15	124	57	5.03	24.47	1.19	0.05
9	1.229	595	62.04	37.24	1.51	2.66	8.97	39	33	9.98	12.06	1.16	0.02
10	1.525	595	42.69	22.71	1.51	2.66	13.54	117	58	5.17	11.84	0.87	0.02
11	2.034	595	37.55	19.29	1.51	2.66	13.28	111	59	4.92	11.54	0.89	0.09
12	2.331	595	35.95	19.45	1.51	2.66	10.96	182	57	3.99	10.93	0.97	0.10
13	0.763	595	67.43	38.31	1.51	2.66	14.87	113	56	4.42	11.71	0.90	0.00
14	0.763	595	70.23	39.60	1.51	2.66	15.99	126	69	9.13	22.46	0.92	0.03
15	0.763	595	81.75	47.82	1.51	2.66	13.12	135	63	9.40	31.43	1.07	0.04
16	1.123	595	58.13	34.59	1.51	2.66	9.55	118	60	9.23	17.93	1.04	0.03
17	1.123	595	64.66	37.76	1.51	2.66	11.97	118	57	9.37	22.36	1.10	0.04
18	1.186	595	57.59	29.85	1.51	2.66	19.13	149	79	3.59	20.04	0.92	0.07
19	1.186	595	52.88	28.98	1.51	2.66	14.70	149	88	3.95	16.45	0.91	0.04
20	1.186	595	64.30	36.57	1.51	2.66	14.31	195	93	3.51	24.52	1.09	0.09
21	0.847	595	69.70	40.25	1.51	2.66	13.64	185	55	3.72	20.71	0.99	0.03
22	0.847	595	51.24	28.32	1.51	2.66	13.83	104	8	7.28	7.33	0.76	0.01
23	1.589	595	32.25	14.83	1.51	2.66	14.35	118	82	4.36	7.24	0.65	0.05
24	0.847	595	63.16	36.41	2.60	2.64	12.98	120	76	4.71	12.53	0.92	0.01
25	0.847	595	66.11	36.30	2.60	2.64	17.48	156	86	4.10	16.57	0.90	0.01
26	0.847	595	72.84	43.20	2.60	2.64	10.93	161	83	4.13	20.88	1.06	0.03
27	0.847	595	105.64	61.10	2.60	2.64	15.39	167	65	4.11	24.98	1.34	0.02
28	1.059	595	62.36	34.80	2.60	2.64	15.48	143	75	4.22	11.91	0.99	0.01
29	1.059	595	54.15	28.78	2.60	2.64	16.77	154	83	4.02	16.63	0.85	0.03
30	1.186	595	59.13	33.26	2.60	2.64	14.30	143	67	3.69	19.77	1.01	0.03
31	1.186	595	67.08	38.56	2.60	2.64	13.76	148	74	3.57	23.71	1.14	0.02
32	1.483	595	39.34	18.73	2.60	2.64	16.36	176	88	3.45	10.96	0.73	0.02
33	1.483	595	46.74	24.88	2.60	2.64	14.66	136	80	3.52	15.45	0.91	0.03
34	1.483	595	53.25	28.81	2.60	2.64	15.54	186	72	3.39	19.73	1.01	0.04
35	1.483	595	59.57	32.28	2.60	2.64	16.95	184	79	3.42	23.61	1.10	0.07
36	1.653	595	38.51	16.34	2.60	2.64	19.13	134	82	3.75	11.36	0.69	0.03
37	1.653	595	46.08	23.02	2.60	2.64	17.21	141	84	3.76	15.96	0.90	0.09
38	1.653	595	52.56	28.02	2.60	2.64	16.18	146	70	3.71	20.08	1.04	0.12
39	1.653	595	59.13	33.13	2.60	2.64	14.58	147	64	3.64	23.79	1.19	0.12
40	1.568	595	38.73	18.76	0.47	2.66	15.60	135	87	3.64	11.58	0.76	0.06
41	1.568	595	46.16	24.41	0.47	2.66	14.80	142	81	3.73	15.96	0.92	0.08
42	1.568	595	53.90	29.62	0.47	2.66	14.77	146	87	3.66	20.35	1.07	0.09
43	1.568	595	59.10	34.08	0.47	2.66	12.39	151	81	3.75	24.25	1.20	0.13
44	1.822	595	37.55	18.70	0.47	2.66	14.29	140	87	4.06	11.92	0.82	0.09
45	1.822	595	45.29	22.96	0.47	2.66	16.33	148	88	4.00	16.48	0.95	0.13
46	1.822	595	51.59	29.70	0.47	2.66	11.33	152	81	3.95	20.87	1.17	0.14
47	2.034	595	35.08	19.49	0.47	2.66	9.71	121	84	3.97	10.64	0.92	0.15
48	2.034	595	42.85	24.99	0.47	2.66	9.05	161	89	3.26	14.75	1.11	0.13
49	2.034	595	50.35	30.68	0.47	2.66	6.79	7	78	3.56	20.07	1.32	0.14
50	2.034	595	54.22	33.47	0.47	2.66	5.64	178	60	3.56	23.79	1.42	0.21
51	2.246	595	34.90	21.54	0.47	2.66	4.68	127	75	4.36	11.38	1.09	0.13
52	2.246	595	42.64	25.31	0.47	2.66	7.95	159	77	3.78	15.90	1.19	0.15
53	2.246	595	35.17	17.28	2.60	2.64	13.82	131	78	4.07	11.19	0.86	0.10
54	2.246	595	42.78	22.75	2.60	2.64	13.58	142	88	3.62	15.55	1.06	0.14
55	2.246	595	47.24	27.46	2.60	2.64	9.96	146	85	3.62	19.82	1.24	0.17
56	2.246	595	52.77	31.74	2.60	2.64	8.10	142	79	3.72	23.74	1.40	0.18
57	2.076	595	36.93	19.14	2.60	2.64	12.77	136	85	3.90	11.87	0.90	0.09
58	2.076	595	43.16	24.38	2.60	2.64	10.84	11	77	3.69	16.02	1.09	0.12
59	2.076	595	50.20	28.50	2.60	2.64	11.99	153	92	3.67	20.34	1.21	0.14
60	2.076	595	54.70	32.31	2.60	2.64	9.85	154	79	3.79	24.16	1.35	0.14
61	1.822	595	36.34	17.74	2.60	2.64	14.46	123	84	3.54	10.84	0.79	0.04
62	1.822	595	43.56	25.20	2.60	2.64	9.63	162	85	3.20	15.12	1.05	0.12
63	1.822	595	50.97	30.34	2.60	2.64	8.79	171	78	3.18	19.05	1.21	0.09
64	1.822	595	56.21	32.54	2.60	2.64	11.66	168	87	3.25	23.71	1.25	0.11
65	0.644	209	34.99	20.17	2.60	2.64	5.60	101	18	0.08	3.80	0.55	0.02
66	0.644	209	49.27	27.29	2.60	2.64	8.22	101	16	0.01	6.60	0.68	0.02
67	0.644	209	51.63	27.99	2.60	2.64	9.89	101	14	0.02	6.84	0.68	0.02
68	0.644	209	28.15	16.32	2.60	2.64	4.98	101	20	0.14	1.99	0.48	0.01
69	0.644	209	30.78	16.70	2.60	2.64	7.96	101	19	0.11	2.45	0.47	0.00
70	0.644	209	40.49	23.10	2.60	2.64	6.26	101	17	0.08	4.73	0.61	0.02
71	0.644	209	53.26	29.33	2.60	2.64	8.49	101	15	0.02	7.37	0.71	0.03
72	0.644	209	35.58	20.28	2.60	2.64	6.26	101	20	0.12	3.62	0.55	0.01
73	0.644	209	40.61	23.32	2.60	2.64	5.82	101	18	0.06	4.58	0.62	0.02

(*Continued*)

Table 1. (Continued).

Run no.	S_o (%)	D (mm)	Y (mm)	R (mm)	d (mm)	SG (-)	y_s (mm)	t_b (s)	t_p (s)	Q_b (l s^{-1})	Q_p (l s^{-1})	V_f (m s^{-1})	V_s (m s^{-1})
74	0.644	209	45.95	25.29	2.60	2.64	8.76	101	17	0.03	5.42	0.64	0.01
75	0.644	209	52.17	28.92	2.60	2.64	7.96	101	16	0.03	7.22	0.71	0.03
76	0.644	209	29.87	16.87	2.60	2.64	6.26	101	21	0.11	2.06	0.48	0.01
77	0.644	209	33.61	19.44	2.60	2.64	5.39	101	19	0.10	2.75	0.54	0.01
78	0.644	209	44.28	24.82	2.60	2.64	7.45	101	18	0.02	5.17	0.64	0.02
79	0.644	209	47.12	26.13	2.60	2.64	8.22	101	18	0.01	5.90	0.66	0.02
80	0.644	209	38.03	21.54	2.60	2.64	6.72	101	19	0.08	3.80	0.58	0.01
81	0.644	209	41.49	23.59	2.60	2.64	6.49	101	18	0.05	4.59	0.62	0.02
82	0.644	209	43.13	23.90	2.60	2.64	8.22	101	17	0.04	5.55	0.61	0.01
83	0.644	209	44.99	24.43	2.60	2.64	9.60	101	16	0.02	6.11	0.62	0.02
84	0.644	209	38.93	21.05	2.60	2.64	9.31	101	18	0.04	4.51	0.55	0.01
85	0.644	209	47.10	25.93	2.60	2.64	8.76	101	17	0.02	5.83	0.65	0.01
86	0.644	209	38.30	22.59	0.47	2.66	3.91	101	17	0.10	4.36	0.62	0.06
87	0.644	209	51.25	29.60	0.47	2.66	3.68	101	16	0.00	7.36	0.76	0.11
88	0.644	209	52.44	29.99	0.47	2.66	4.65	101	15	0.01	7.64	0.75	0.10
89	0.644	209	29.07	17.09	0.47	2.66	4.40	101	19	0.21	2.22	0.50	0.03
90	0.644	209	33.05	19.59	0.47	2.66	3.91	101	17	0.19	2.65	0.56	0.04
91	0.644	209	41.19	24.21	0.47	2.66	3.86	101	18	0.04	4.99	0.65	0.08
92	0.644	209	56.85	32.46	0.47	2.66	3.51	101	15	0.00	8.02	0.81	0.13
93	0.644	209	39.63	23.20	0.47	2.66	4.40	101	17	0.07	4.08	0.62	0.05
94	0.644	209	43.42	25.52	0.47	2.66	3.46	101	17	0.08	4.99	0.68	0.06
95	0.644	209	47.40	27.47	0.47	2.66	4.21	101	16	0.04	5.56	0.71	0.07
96	0.644	209	30.86	18.45	0.47	2.66	3.46	101	19	0.32	2.08	0.54	0.03
97	0.644	209	32.77	19.21	0.47	2.66	4.59	101	20	0.11	2.80	0.54	0.04
98	0.644	209	42.21	24.97	0.47	2.66	3.03	101	19	0.41	4.22	0.67	0.06
99	0.644	209	37.41	21.71	0.47	2.66	5.18	101	19	0.09	3.79	0.59	0.05
100	0.644	209	41.66	24.19	0.47	2.66	4.86	101	17	0.07	4.63	0.64	0.05
101	0.644	209	43.34	25.14	0.47	2.66	4.78	101	18	0.06	5.71	0.66	0.06
102	0.644	209	48.65	28.13	0.47	2.66	4.21	101	16	0.03	6.67	0.72	0.09
103	0.644	209	36.32	21.27	0.35	2.65	4.59	101	18	0.06	4.24	0.58	0.05
104	0.644	209	51.00	29.01	0.35	2.65	5.60	101	15	0.01	6.81	0.73	0.08
105	0.644	209	50.99	29.11	0.35	2.65	5.18	101	15	0.01	6.90	0.73	0.09
106	0.644	209	28.62	16.45	0.35	2.65	5.39	101	18	0.23	2.00	0.48	0.02
107	0.644	209	32.66	18.92	0.35	2.65	5.26	101	17	0.19	2.67	0.53	0.03
108	0.644	209	42.79	24.72	0.35	2.65	5.18	101	16	0.07	4.80	0.65	0.04
109	0.644	209	54.41	30.76	0.35	2.65	5.60	101	17	0.00	7.36	0.76	0.07
110	0.644	209	37.13	21.55	0.35	2.65	5.18	101	18	0.10	3.75	0.59	0.03
111	0.644	209	41.56	24.21	0.35	2.65	4.59	101	17	0.08	4.71	0.64	0.05
112	0.644	209	45.08	25.81	0.35	2.65	5.73	101	17	0.07	5.47	0.67	0.05
113	0.644	209	54.08	30.60	0.35	2.65	5.60	101	15	0.03	7.31	0.76	0.08
114	0.644	209	29.46	16.96	0.35	2.65	5.39	101	20	0.19	2.02	0.49	0.03
115	0.644	209	33.04	18.92	0.35	2.65	5.90	101	19	0.13	2.74	0.53	0.03
116	0.644	209	44.81	25.64	0.35	2.65	5.82	101	17	0.04	5.18	0.66	0.04
117	0.644	209	48.43	27.71	0.35	2.65	5.39	101	17	0.02	5.88	0.70	0.05
118	0.644	209	39.31	22.65	0.35	2.65	5.60	101	18	0.09	3.92	0.60	0.04
119	0.644	209	41.99	24.16	0.35	2.65	5.60	101	17	0.08	4.59	0.63	0.04
120	0.644	209	43.59	25.04	0.35	2.65	5.60	101	18	0.04	5.64	0.65	0.04
121	0.644	209	44.65	25.62	0.35	2.65	5.60	101	17	0.06	6.12	0.66	0.07

- Figure 5(e) shows the inversely proportional relationship between V_s/V_f and the dimensionless parameter Q_b/Q_p, meaning that higher and steeper discharge hydrographs (i.e. lower ratios Q_b/Q_p) show higher V_s/V_f values.
- In general, based on what was previously mentioned, higher values of S_o and R and lower values of d, SG, and Q_b/Q_p lead to higher sediment velocities V_s.

3.2. Evolutionary polynomial regression model

A new regression-based model was developed here to predict the dimensionless ratio V_s/V_f during flushing operation. The new model includes the group of parameters identified in previous studies (Ab Ghani and Azamathulla 2011; Ebtehaj and Bonakdari 2016; May et al. 1996; Montes, Kapelan, and Saldarriaga 2021) and the graphic analysis carried out for the experimentally collected data, as shown in Figure 5.

Evolutionary polynomial regression (EPR) is a hybrid regression technique that combines numerical and symbolic regression (Giustolisi and Savic 2006, 2004). In its original formulation, it used single-objective genetic algorithms to explore the formula space, and then it estimates the least-squares regression coefficients. This technique has proved to be effective when the number of polynomial terms is not large (Giustolisi and Savic 2009). To solve these issues, Giustolisi and Savic (Giustolisi and Savic 2009) introduced the EPR technique combined with a Multi-Objective Genetic Algorithm (MOGA). This novel technique maximises the model accuracy (i.e. minimises the sum of squared errors) and minimises the number of polynomial coefficients, and therefore improves the exploration of the space of

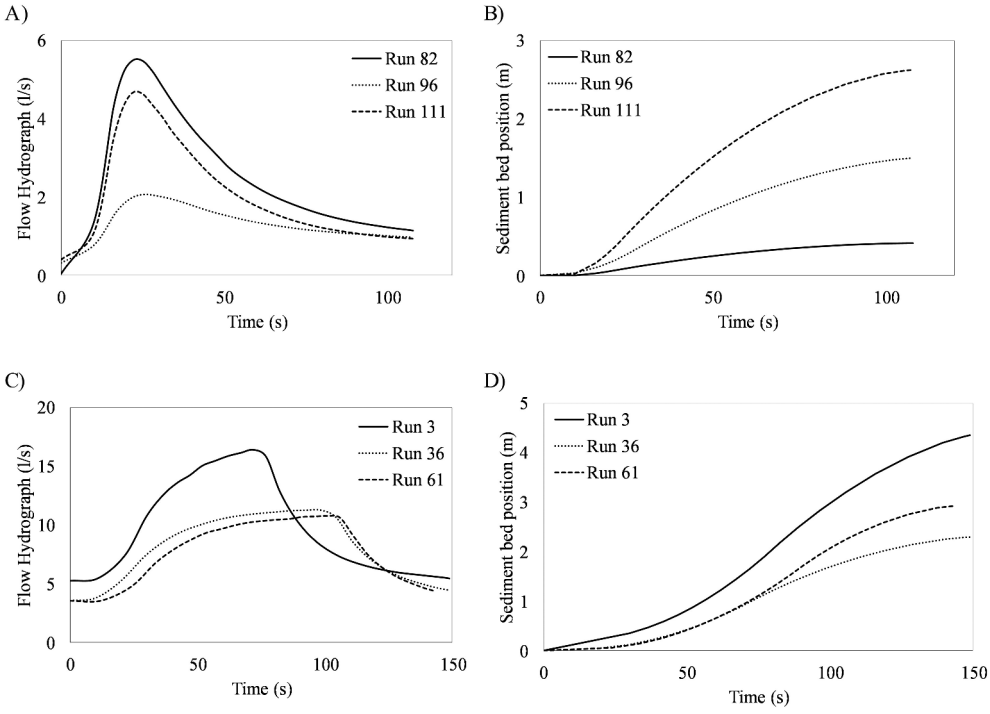

Figure 4. Example of flow hydrographs and sediment bed position for several experiments shown in Table 1.

symbolic formulas. EPR-MOGA considers some pseudo-polynomial expressions such as (Giustolisi and Savic 2009):

$$\hat{Y} = a_0 + \sum_{j=1}^{m} a_j (\boldsymbol{X}_1)^{ES(j,1)} \cdot \ldots \cdot (\boldsymbol{X}_k)^{ES(j,k)} \cdot f\left((\boldsymbol{X}_1)^{ES(j,k+1)}\right) \cdot \ldots \cdot f\left((\boldsymbol{X}_k)^{ES(j,2k)}\right) \tag{5}$$

where $\hat{Y}$ is the vector of model predictions; ES and j the matrix of candidate exponents and the inner function, respectively, both selected by the user; m the number of terms; a_0 the bias term; a_j the adjustable parameters estimated by linear least squares and $\boldsymbol{X_j}$ the candidate explanatory variables. The inner function f defined by the user can be logarithmic, exponential, tangent hyperbolic, or secant hyperbolic, and must be selected according to the physics of the problem studied. The EPR technique returns a range of models showing the influence of different explanatory factors by progressively adding these as input variables to monomial formulas, starting from the most important ones. For each EPR identified model, the following performance indices are calculated: the Bayesian Information Criterion (*BIC*) and the Coefficient of Determination (R^2), as shown in Equations (6) and (7), respectively.

$$BIC = \left(1 + d\frac{\log(n)}{n}\right)\left(\sum_{i=1}^{n}(Y^* - Y)^2\right) \tag{6}$$

$$R^2 = 1 - \frac{\sum_{i=1}^{n}(Y^* - Y)^2}{\sum_{i=1}^{n}\left(Y^* - \overline{Y^*}\right)^2} \tag{7}$$

where Y^* and Y are the observed and calculated data, respectively, n is the number of data, d the number of parameters included in the model and $\overline{Y^*}$ the mean of observed data. The Coefficient of Determination measures the fraction of variance that can be explained. Note that this coefficient varies between 0 and 1, where 1 denotes a perfect match between observed and calculated data. The Bayesian Information Criterion measures the trade-off between accuracy and parsimony of the model. This measure penalises formulas with large number of parameters. The model with the lowest BIC value is selected as optimal.

The new model was constructed to predict the dimensionless relation V_s/V_f, i.e., the vector of model predictions $\hat{Y}$ is defined as V_s/V_f. The matrix of candidate exponents was defined with values ranging from −2.50 to 2.50, considering steps of 0.1, i.e. $ES = [-2.50, -1.40, \ldots, 1.40, 2.50]$. The matrix of candidate explanatory variables is defined as follows:

$$\boldsymbol{X_j} = \left[\psi, \frac{d}{-}, \frac{Q_b}{Q_p}, \frac{y_s}{R}, \frac{t_b}{t_p}, \beta\right] \tag{8}$$

Using previous considerations, and randomly splitting the experimental data collected on the 209 mm and 595 mm pipes, for both training (75% of the data) and testing (25% of the data) stages, the results shown in Table 2 were obtained using the EPR-MOGA strategy.

Table 2 shows the Pareto front (i.e. range of models) generated by the EPR, together with the corresponding *BIC* and R^2 values. For example, the best one input variable model includes only the Shields parameter as an explanatory variable for predicting the V_s/V_f ($V_s/V_f = 0.17\psi^{0.5}$). This is the least complex, i.e., most parsimonious model hence, unsurprisingly, it has a rather low prediction accuracy (*BIC* = −48.21 and R^2 = 0.38). In contrast, the

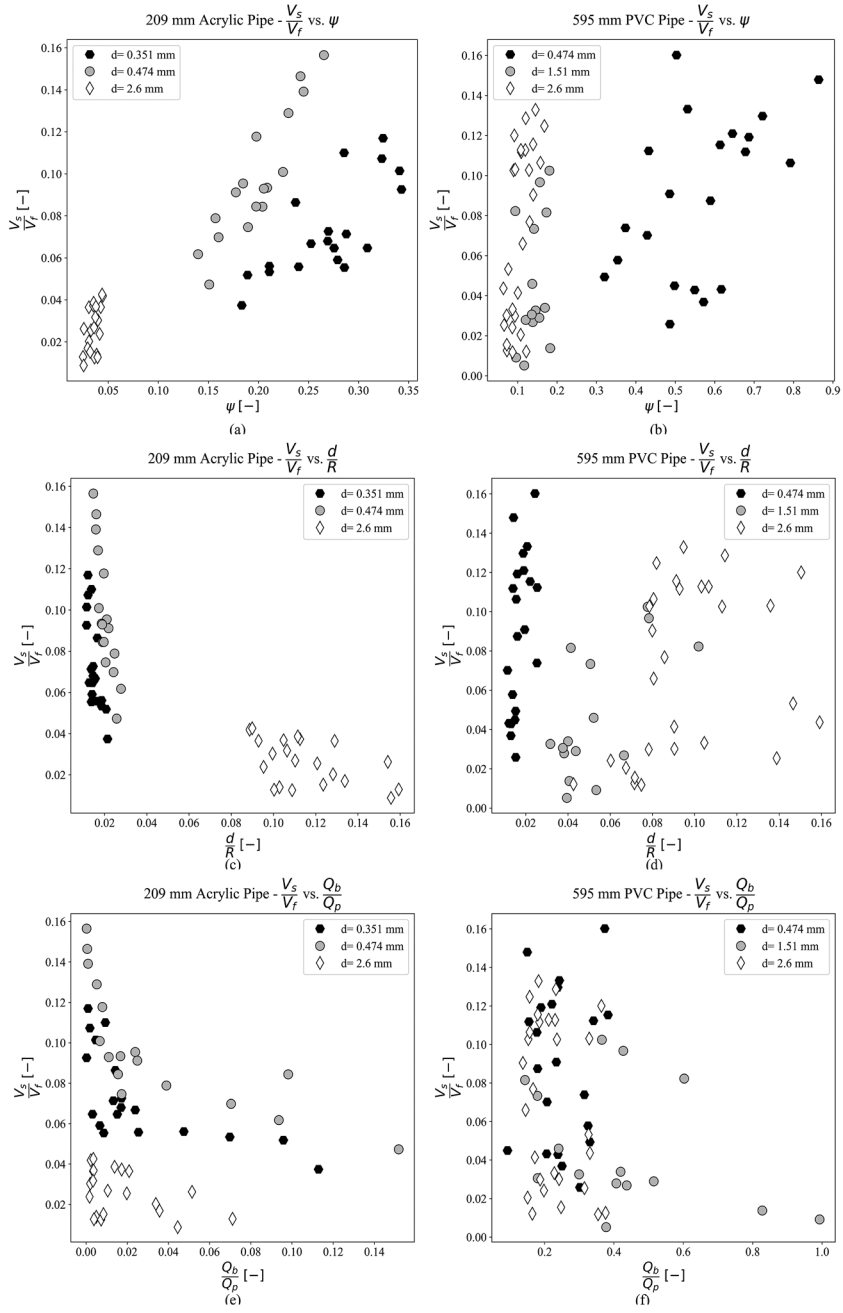

Figure 5. Plots showing the relationships between the dimensionless velocity (V_s/V_f) and other dimensionless variables in both acrylic and PVC pipe. Clustered results by particle diameter.

Table 2. Pareto solution provided by the EPR-MOGA strategy.

	Terms of monomial formula							Performance Index	
Number of inputs	Coefficient (a_j)	ψ	$\frac{Q_b}{Q_p}$	$\frac{d}{R}$	$\frac{y_s}{R}$	$\frac{t_b}{t_p}$	β	*BIC*	R^2
1	0.17	0.50	-	-	-	-	-	−48.21	0.38
2	0.14	0.60	−0.10	-	-	-	-	−66.19	0.48
3	8.13	1.40	−0.30	0.90	-	-	-	−104.55	0.63
4	11.47	1.50	−0.30	1.00	0.10	-	-	−100.56	0.64
5	121.48	2.10	−0.20	1.60	0.80	0.10	-	−96.49	0.64
6	2.48	1.40	−0.30	0.90	0.10	−0.20	1.00	−92.22	0.64

6-variable model includes all candidate explanatory factors $\left(V_s/V_f = 2.48\psi^{1.4}\left(\frac{Q_b}{Q_p}\right)^{-0.3}\left(\frac{d}{R}\right)^{0.9}\left(\frac{y_s}{R}\right)^{0.1}\left(\frac{t_b}{t_p}\right)^{-0.2}\beta\right)$, resulting in low parsimony model but with improved prediction accuracy (*BIC* = −92.22 and R^2 = 0.64). Based on this, the model that shows the best trade-off between accuracy and parsimony is the model with three input variables. This model is shown in Equation (9).

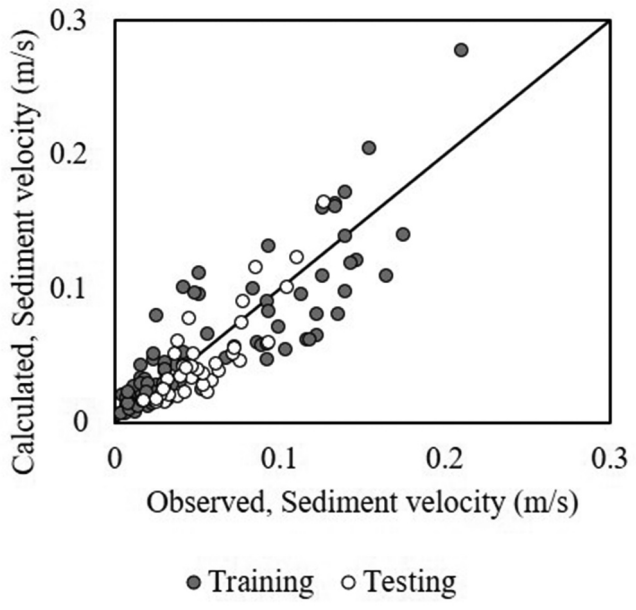

Figure 6. EPR-MOGA model accuracy for both training and testing stage.

$$\frac{V_s}{V_f} = 8.13\left(\frac{d}{R}\right)^{0.90}\left(\frac{RS_o}{(SG-1)d}\right)^{1.40}\left(\frac{Q_b}{Q_p}\right)^{-0.30} \quad (9)$$

Or rearranging the above formula to simplify the d/R term:

$$\frac{V_s}{V_f} = 8.13\left(\frac{d}{R}\right)^{-0.50}\left(\frac{S_o}{(SG-1)}\right)^{1.40}\left(\frac{Q_b}{Q_p}\right)^{-0.30} \quad (10)$$

The obtained model was used to estimate the flushing efficiency in larger pipes considering different flow conditions and sediment characteristics. Further details are described in the section below. The model's accuracy can be seen in Figure 6 for both training and testing datasets.

As it can be seen from the above equation and figure, Equation (10) is consistent with the graphical analysis presented in Figure 6. Further, it can be seen from the model obtained that $\frac{S_o}{(SG-1)}$ is the most important feature for predicting the sediment velocity during the flushing cleaning operation – the more the pipe slope increases, the higher the particle velocity is (note that the $\frac{S_o}{(SG-1)}$ parameter comes from the Shields parameter). The Shields parameter shows the ratio

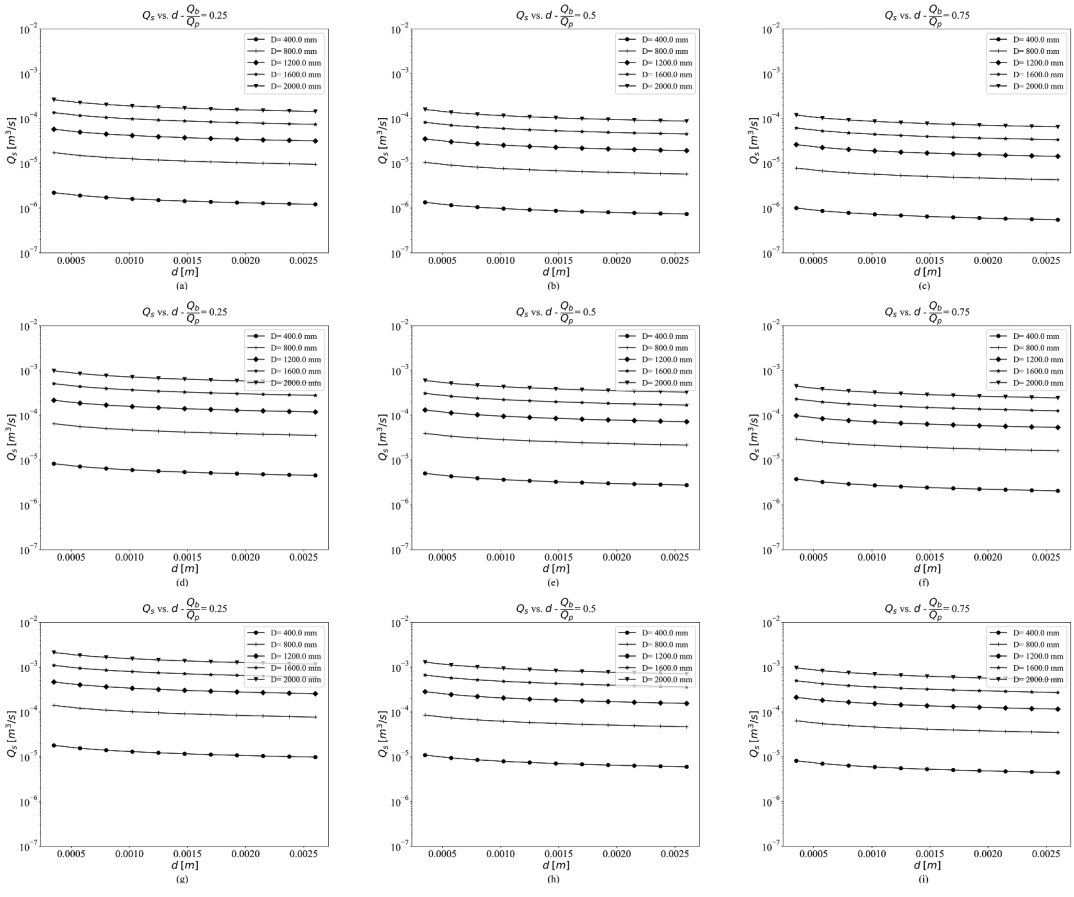

Figure 7. Efficiency of flushing discharge vs particle diameter for several base and peak flow relations ($0.25 < Q_b/Q_p < 0.75$) and pipe slope: a), b) and c) $S_o = 0.5\%$; d), e) and f) $S_o = 1.0\%$ and g), h) and i) $S_o = 1.5\%$.

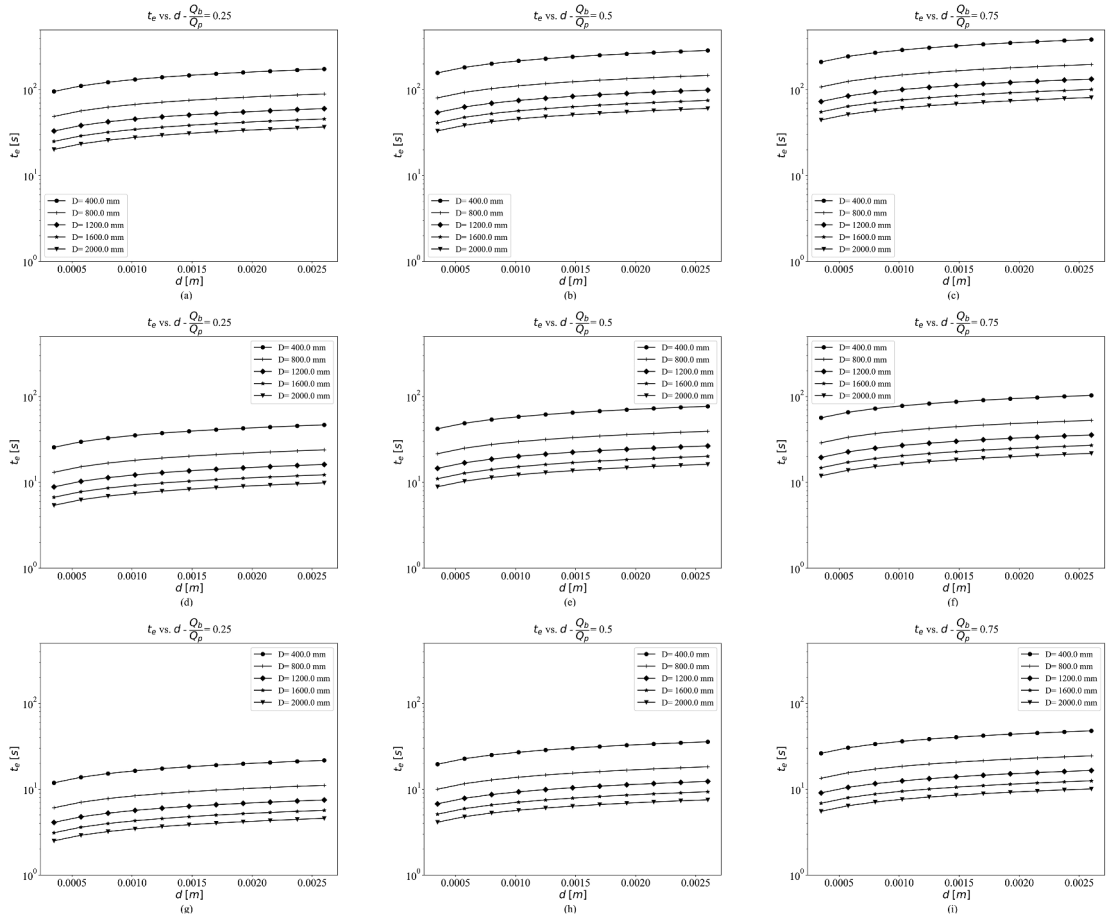

Figure 8. Flushing time vs particle diameter for several base and peak flow relations ($0.25 < Q_b/Q_p < 0.75$) and pipe slope: a), b) and c) $S_o = 0.5\%$; d), e) and f) $S_o = 1.0\%$ and g), h) and i) $S_o = 1.5\%$.

between the hydrodynamic forces acting on the particles and the resistance due to gravity. This parameter has been identified as one of the most relevant for predicting the incipient motion in sewers (Delleur 2001; Safari, Mohammadi, and Ab Ghani 2018; Wan Mohtar et al. 2018). As mentioned above, V_s/V_f is inversely proportional to d/R, which is consistent with the results shown by EPR-MOGA model.

4. Results and discussion

The new model shown in Equation (10) was used to generate charts to estimate flushing efficiency as a function of the characteristics of the discharged hydrograph, the pipe geometry and the sediment properties. In this context, two flushing-efficiency measures were defined as a function of the area of deposited bed (A_s) and the sediment velocity. The first measure, Q_s, is the volume of sediment removed by unit time (i.e. the sediment flow rate = A_sV_s). The second measure, t_e, is the flushing time required to clean 1.0 m of the pipe (= $1/V_s$). Figures 7 and 8 were constructed for several pipe diameters using previous measures. To construct these figures, the less-significant variables identified by the EPR-MOGA model (as shown in Table 2) remained constant. The sediment thickness was defined as $y_s/D = 1\%$, the specific gravity of the sediments as 2.6, and the relation between the base and peak time of the hydrograph as $t_b/t_p = 5.0$.

The following observations can be made from Figures 7 and 8:

- Q_s is inversely proportional to d and Q_b/Q_p. In addition, Q_s seems to be near-steady for particle diameters greater than 1.5 mm in pipes with diameters less than 800 mm. All above for the same pipe slope and Q_b/Q_p relation. Increasing the pipe slope directly increase the sediment transport rate.
- As the Q_b/Q_p ratio increases, the sediment removal rate decreases. For example, in Figure 7(a), when $Q_b/Q_p = 0.25$ in a 1200 mm diameter pipe containing a deposited sediment bed with $d = 1$ mm, $Q_s = 0.5 \times 10^{-4}$ m^3/s, while for $Q_b/Q_p = 0.75$ the Q_s value changes to 0.2×10^{-4} m^3/s, that is 60% less (as shown in Figure 7(c)).
- Flushing discharges seem to be more efficient in larger sewer pipes. The sediment transport rate can be five times higher in 2000 mm diameter pipes, compared to 1200 mm diameter pipes.
- Figure 8 shows a direct relationship between t_e and d and Q_b/Q_p. Based on this, as d increases and Q_p decreases, the required flushing time to clean 1 meter of the pipe increases. For example, in Figure 8(d) when $Q_b/Q_p = 0.25$ in a 800 mm diameter pipe containing a deposited sediment bed with $d = 1.5$ mm, $t_e = 20$ sec, while for $Q_b/Q_p = 0.75$ the t_e value changes to 45 sec, that is 125% more (as shown in Figure 8(f))

Table 3. Comparison of results for predicting the flushing efficiency in Laplace et al. (2003) case of study.

Reference	Removal rate [kg m^{-3}]	Observations
Laplace et al. (2003)	0.93	Original case of Study reported in a trunk combined sewer in Marseille, France
Dettmar (2007)	-	Volume of water value reported to clean a pipe section of 150 m long. Relevant parameters as pipe slope and particle diameter are not considered.
Bong, Lau, and Ab Ghani (2013)	0.21	Good approximation. Experimental model (Equation (3)) obtained with a constant flume slope of 0.001.
EPR-MOGA Equation (10)	0.4–1.25	Good performance for predicting the removal rate during flushing waves operation. Model consider relevant parameters as the mean particle diameter and the pipe geometry.

- The flushing time decreases as the S_o and D increase. That is, flushing is a more efficient technique in large and steep pipes.

4.1. Model comparison

To test the accuracy of the model shown in Equation (10), the case study described in Laplace et al. (2003) was used. This case study is located in Marseille, France, on a combined sewer network. Specifically, this study considers an ovoid section of 1700 mm, 120 m long with a bottom slope of 0.03%. A near-uniform deposited bed of 140 mm thickness was observed along the entire length of the flume. The deposited bed was characterised as coarser upstream (d = 8 mm) and finer downstream (d = 0.6 mm). Full details are shown in Laplace et al. (2003).

Using a Hydrass-flushing gate located inside the section, a series of flushes were conducted for testing the efficiency on removing the deposited material. During each flush, a total volume of 6.0 m^3 of water was discharged into the pipe. As reported by Laplace et al. (2003), the mass of particles eroded during the first flush was 6.3 kg, i.e., the removal rate was 1.08 kg of material per 1.0 m^3 of water (= 1.08 kg m^{-3}).

Two existing procedures are compared with the new EPR-MOGA model presented in Equation (10): the model proposed by Bong, Lau, and Ab Ghani (2013) (i.e. Equation (3)) and the design tables shown by Dettmar (2007). To compare the results, several initial conditions are defined based on the case study description, which are outlined as follows:

(1) Thickness of the deposited bed (y_s) = 0.14 m
(2) Peak flow during flushing operation (Q_p) = 100 l s^{-1}
(3) Specific gravity of the sediments (SG) = 2.60
(4) Mean particle diameter (d) = 0.6–8.0 mm
(5) Mass of material per meter of pipe = 54.22 kg m^{-1}

According to Bong, Lau, and Ab Ghani (2013), the number of flushes required to move 1 m of deposited material can be estimated by applying Equation (3). For this equation, the number of flushes is only a function of the thickness of the deposited bed. As a result, 42 flushes (= 250.6 m^3 of water) can potentially remove 54.22 kg of the deposited material (i.e. the removal rate is 0.21 kg m^{-3}). Design tables proposed by Dettmar (2007) suggest a flushing volume of 48 m^3 for a basic cleaning of the 150 m long sewer (i.e. a full removing of the deposited material). No removal rates are provided by Dettmar (2007).

Finally, using the new model proposed in this study, a range of removal rates are obtained as a function of the mean particle diameter. Potentially, a flushing volume of 10.18 m^3 can remove 14.5 kg of deposited material with a mean particle diameter of 0.6 mm (i.e. the removal rate is 0.40 kg m^{-3}). By changing the particle size of the deposited material to 8.3 mm, the removal rate is 1.25 kg m^{-3}.

As shown in Table 3, a direct comparison of the method proposed by Dettmar (2007) and the results reported by Laplace et al. (2003) is not possible. However, this method seems to underestimate the real volume required to remove the deposited bed. Relevant parameters such as the mean particle diameter and the sewer hydraulics are not included in this method. Due to the pipe slope in the case of study is almost flat, obtaining minimum shear stress of 5.0 N m^{-2} for cleaning the pipe, according to Dettmar (2007), requires larger flows.

The model presented by Bong, Lau, and Ab Ghani (2013) is a good approach for determining the number of flushes required to move the deposited material. However, because of the non-inclusion of relevant pipe hydraulics and sediment parameters, the results are underestimated, compared to the values reported by Laplace et al. (2003).

4.2. Model considerations

The new model presented here shows good prediction accuracy with the data reported by Laplace et al. (2003). This is explained by the inclusion of relevant parameters for predicting the removal rate during the flushing operation. The model also shows good extrapolation capabilities under different sewer diameters and a wide range of variations of the mean particle diameter.

The Shields parameter was selected as the most important one due to the highest value in the regression coefficient and the Pareto solution provided by the EPR-MOGA strategy. This was expected since this parameter determines the threshold condition of sediment initiation motion. The sediment thickness parameter is less important for defining the sediment velocity during the flushing operation due to the low regression coefficient presented in Table 2. As a result, the model can be used in both combined and storm sewers, where the sediment thickness ranges from 10 mm to 100 mm and 10 mm to 330 mm, respectively (Bong, Lau, and Ab Ghani 2016).

The model includes the peak flow as an explanatory variable for predicting sediment transport rate. Higher peak flow implies a higher removal rate since higher shear stresses are generated at the bottom of the pipe. The observed shear stress values (ranging from 2.0 N/m^2 to 6.5 N/m^2 in the PVC pipe) are consistent with those reported in the literature for the erosion and transport of bed material (Dettmar 2007; Campisano, Creaco,

and Modica 2008; Yang et al. 2019). However, since the model only considers transport as bedload, some fine particles may be eroded and transported in suspension (which has been identified as one of the major sources of pollution in CSO (Laplace et al. 2003; Saul et al. 2003)), due to the high turbulence of the flow. This is particularly important in well-graded materials where wide ranges of mean particle sizes are present.

Even though the new model was developed considering a wide range of variations in input variables, some limitations exist. The granular material used in the experiments cannot represent the cohesive properties of sediments found in real sewer systems. As a result, an increased bed resistance to erosion can be seen in practice (Campisano et al. 2019). In addition, the lowest pipe slope value considered during the tests was 0.644%, which is higher than the minimum self-cleansing value recommended in several industry design codes and water utilities design manuals (e.g. Health Research Inc (2004), as quoted by Montes et al. (2019)).

5. Conclusions

This study proposes a simple model to predict the sediment transport rate in practice based on data collected from a set of 121 lab experiments conducted on a 209 mm diameter acrylic pipe and 595 mm diameter PVC pipe. The data collected this way were processed using the EPR-MOGA modelling technique. A new model for predicting the sediment velocity during flushing operation was developed and used for constructing design charts. Based on the results obtained, the following conclusions are made:

(1) The new model developed and presented here can predict the sediment transport rate during flushing discharges accurately in practice. This model includes the group of parameters that most affect the flushing efficiency in sewer pipes.
(2) The sediment transport rate is principally affected by four parameters: pipe slope, pipe diameter, particle diameter and discharged peak flow. In pipes with large diameters and slopes, the flushing is more effective. This is because of the high regression exponents for both $\frac{S_o}{(SG-1)}$ and d/R variables obtained in the EPR-MOGA model presented here. The sediment transport is not significantly affected by the value of the deposited sediment thickness.
(3) The new model proposed outperforms the simplified models and methods reported in the literature in terms of removal sediment rate prediction. This is seen by the better prediction accuracy shown when compared to the case study reported by Laplace et al. (2003).
(4) Existing models such as Bong, Lau, and Ab Ghani (2013) and Dettmar (2007) for predicting sediment transport tend to underestimate the total volume of water required to clean a deposited sediment bed. The EPR-MOGA model is more accurate in predicting the sediment transport rate as this model includes parameters affecting the flushing efficiency, such as flushing hydraulics, pipe geometry and sediment properties.

Based on the conclusions mentioned above, the new flushing model can be useful for designing flushing schemes during the operational stage of existing sewer pipes in engineering practice. Further research is recommended to test the model proposed in real sewer pipes under different sediment (i.e. cohesive materials) and hydraulic conditions.

Acknowledgement

The authors would like to thank Professor Orazio Giustolisi who developed and made available for free the EPR-MOGA XL software used in this research.

Disclosure statement

No potential conflict of interest was reported by the author(s).

ORCID

Carlos Montes http://orcid.org/0000-0003-0758-4697
Sergio Vanegas http://orcid.org/0000-0001-5786-9450
Zoran Kapelan http://orcid.org/0000-0002-0934-4470
Luigi Berardi http://orcid.org/0000-0002-6252-2467
Juan Saldarriaga http://orcid.org/0000-0003-1265-2949

References

Ab Ghani, A., and H. Azamathulla. 2011. "Gene-Expression Programming for Sediment Transport in Sewer Pipe Systems." *Journal of Pipeline Systems Engineering and Practice* 2 (3): 102–106. doi:10.1061/(ASCE)PS.1949-1204.0000076.

Ashley, R., J. Bertrand-Krajewski, T. Hvitved-Jacobsen, and M. Verbanck. 2004. *Solids in Sewers: Characteristics, Effects and Control of Sewer Solids and Associated Pollutants*. London: IWA Publishing. doi:10.2166/9781780402727.

ASTM D854-14. 2014. *Standard Test Methods for Specific Gravity of Soil Solids by Water Pycnometer*. West Conshohocken, PA: ASTM International.

Bajirao, T., P. Kumar, M. Kumar, A. Elbeltagi, and A. Kuriqi. 2021. "Superiority of Hybrid Soft Computing Models in Daily Suspended Sediment Estimation in Highly Dynamic Rivers." *Sustainability* 13 (2): 542. doi:10.3390/su13020542.

Bertrand-Krajewski, J., J. Bardin, C. Gibello, and D. Laplace. 2003. "Hydraulics of a Sewer Flushing Gate." *Water Science and Technology* 47 (4): 129–136. doi:10.2166/wst.2003.0237.

Bong, C., T. Lau, and A. Ab Ghani. 2013. "Hydraulics Characteristics of Tipping Sediment Flushing Gate." *Water Science and Technology* 68 (11): 2397–2406. doi:10.2166/wst.2013.498.

Bong, C., T. Lau, and A. Ab Ghani. 2016. "Potential of Tipping Flush Gate for Sedimentation Management in Open Stormwater Sewer." *Urban Water Journal* 13 (5): 486–498. doi:10.1080/1573062X.2014.994002.

Campisano, A., and C. Modica. 2003. "Flow Velocities and Shear Stresses during Flushing Operations in Sewer Collectors." *Water Science and Technology* 47 (4): 123–128. doi:10.2166/wst.2003.0236.

Campisano, A., C. Modica, E. Creaco, and G. Shahsavari. 2019. "A Model for Non-uniform Sediment Transport Induced by Flushing in Sewer Channels." *Water Research* 163: 114903. doi:10.1016/j.watres.2019.114903.

Campisano, A., E. Creaco, and C. Modica. 2004. "Experimental and Numerical Analysis of the Scouring Effects of Flushing Waves on Sediment Deposits." *Journal of Hydrology* 299 (3–4): 324–334. doi:10.1016/j.jhydrol.2004.08.009.

Campisano, A., E. Creaco, and C. Modica. 2006. "Experimental Analysis of the Hydrass Flushing Gate and Laboratory Validation of Flush Propagation

Modelling." *Water Science and Technology* 54 (6–7): 101–108. doi:10.2166/wst.2006.608.

Campisano, A., E. Creaco, and C. Modica. 2007. "Dimensionless Approach for the Design of Flushing Gates in Sewer Channels." *Journal of Hydraulic Engineering* 133 (8): 964–972. doi:10.1061/(ASCE)0733-9429(2007)133:8(964).

Campisano, A., E. Creaco, and C. Modica. 2008. "Laboratory Investigation on the Effects of Flushes on Cohesive Sediment Beds." *Urban Water Journal* 5 (1): 3–14. doi:10.1080/15730620701726259.

Caviedes-Voullième, D., M. Morales-Hernández, C. Juez, A. Lacasta, and P. García-Navarro. 2017. "Two-dimensional Numerical Simulation of Bed-load Transport of a Finite-depth Sediment Layer: Applications to Channel Flushing." *Journal of Hydraulic Engineering* 143 (9): 04017034. doi:10.1061/(ASCE)HY.1943-7900.0001337.

Chebbo, G., D. Laplace, A. Bachoc, Y. Sanchez, and B. Le Guennec. 1996. "Technical Solutions Envisaged in Managing Solids in Combined Sewer Networks." *Water Science and Technology* 33 (9): 237–244. doi:10.1016/0273-1223(96)00392-7.

Creaco, E., and J. Bertrand-Krajewski. 2009. "Numerical Simulation of Flushing Effect on Sewer Sediments and Comparison of Four Sediment Transport Formulas." *Journal of Hydraulic Research* 47 (2): 195–202. doi:10.3826/jhr.2009.3363.

De Sutter, R., M. Huygens, and R. Verhoeven. 1999. "Unsteady Flow Sediment Transport in a Sewer Model." *Water Science and Technology* 39 (9): 121–128. doi:10.1016/S0273-1223(99)00224-3.

Delleur, J. 2001. "New Results and Research Needs on Sediment Movement in Urban Drainage." *Journal of Water Resources Planning and Management* 127 (3): 186–193. doi:10.1061/(ASCE)0733-9496(2001)127:3(186).

Dettmar, J. 2005. "Beitrag zur Verbesserung der Reinigung von Abwasserkanälen." PhD diss., RWTH Aachen University.

Dettmar, J. 2007. "A New Planning Procedure for Sewer Flushing." Paper presented at the NOVATECH 2007 – Sixth International Conference on Sustainable Techniques and Strategies in Urban Water Management, Lyon, June 25–28.

Dettmar, J., B. Rietsch, and U. Lorenz. 2002. "Performance and Operation of Flushing Devices - Results of a Field and Laboratory Study." *Global Solutions for Urban Drainage: Proceedings of the Ninth International Conference on Urban Drainage* 1–10. doi:10.1061/40644-(2002)291.

Ebtehaj, I., and H. Bonakdari. 2016. "Bed Load Sediment Transport in Sewers at Limit of Deposition." *Scientia Iranica* 23 (3): 907–917. doi:10.24200/sci.2016.2169.

Ebtehaj, I., H. Bonakdari, S. Shamshirband, Z. Ismail, and R. Hashim. 2017. "New Approach to Estimate Velocity at Limit of Deposition in Storm Sewers Using Vector Machine Coupled with Firefly Algorithm." *Journal of Pipeline Systems Engineering and Practice* 8 (2): 04016018. doi:10.1061/(ASCE)PS.1949-1204.0000252.

Fan, C. 2004. *Sewer Sediment and Control A Management Practices Reference Guide, EPA/600/R-04/059*. Washington, DC: U.S. Environmental Protection Agency.

Fan, C., R. Field, W. Pisano, J. Barsanti, J. Joyce, and H. Sorenson. 2001. "Sewer and Tank Flushing for Sediment, Corrosion, and Pollution Control." *Journal of Water Resources Planning and Management* 127 (3): 194–201. doi:10.1061/(ASCE)0733-9496(2001)127:3(194).

Giustolisi, O., and D. Savic. 2004. "A Novel Genetic Programming Strategy: Evolutionary Polynomial Regression." *Proceedings of the 6th International Conference on Hydroinformatics* 787–794. doi:10.1142/9789812702838_0097.

Giustolisi, O., and D. Savic. 2006. "A Symbolic Data-driven Technique Based on Evolutionary Polynomial Regression." *Journal of Hydroinformatics* 8 (4): 207–222. doi:10.2166/hydro.2006.020.

Giustolisi, O., and D. Savic. 2009. "Advances in Data-driven Analyses and Modelling Using EPR-MOGA." *Journal of Hydroinformatics* 11 (3–4): 225–236. doi:10.2166/hydro.2009.017.

Guo, Q., C. Fan, R. Raghaven, and R. Field. 2004. "Gate and Vacuum Flushing of Sewer Sediment: Laboratory Testing." *Journal of Hydraulic Engineering* 130 (5): 463–466. doi:10.1061/(ASCE)0733-9429(2004)130:5(463).

Health Research Inc. 2004. "Recommended Standards for Wastewater Facilities." *A Report of the Wastewater Committee* 12224 (518): 1–102.

Khosravi, K., J. Cooper, P. Daggupati, B. Thai Pham, and D. Tien Bui. 2020. "Bedload Transport Rate Prediction: Application of Novel Hybrid Data Mining Techniques." *Journal of Hydrology* 585: 124774. doi:10.1016/j.jhydrol.2020.124774.

Kuriqui, A., G. Koçileri, and M. Ardiçlioğlu. 2020. "Potential of Meyer-Peter and Müller Approach for Estimation of Bed-load Sediment Transport under Different Hydraulic Regimes." *Modeling Earth Systems and Environment* 6: 129–137. doi:10.1007/s40808-019-00665-0.

Lainé, S., L. Phan, D. Malabat, and B. Duffros. 1998. "Flush Cleaning of Sewer Using the Hydras-Valve." Paper presented at the 4th International Conference on Urban Drainage Modelling, London, September 21–24.

Laplace, D., C. Oms, M. Ahyerre, G. Chebbo, J. Lemasson, and L. Felouzis. 2003. "Removal of the Organic Surface Layer in Combined Sewer Sediment Using a Flushing Gate." *Water Science and Technology* 47 (4): 19–26. doi:10.2166/wst.2003.0211.

May, R., J. Ackers, D. Butler, and S. John. 1996. "Development of Design Methodology for Self-cleansing Sewers." *Water Science and Technology* 33 (9): 195–205. doi:10.1016/0273-1223(96)00387-3.

Montes, C., J. Bohorquez, S. Borda, and J. Saldarriaga. 2019. "Impact of Self-Cleansing Criteria Choice on the Optimal Design of Sewer Networks in South America." *Water (Switzerland)* 11 (6): 1148. doi:10.3390/w11061148.

Montes, C., L. Berardi, Z. Kapelan, and J. Saldarriaga. 2020a. "Predicting Bedload Sediment Transport of Non-cohesive Material in Sewer Pipes Using Evolutionary Polynomial Regression – Multi-objective Genetic Algorithm Strategy." *Urban Water Journal* 17 (2): 154–162. doi:10.1080/1573062X.2020.1748210.

Montes, C., S. Vanegas, Z. Kapelan, L. Berardi, and J. Saldarriaga. 2020b. "Non-deposition Self-cleansing Models for Large Sewer Pipes." *Water Science and Technology* 81 (3): 606–621. doi:10.2166/wst.2020.154.

Montes, C., Z. Kapelan, and J. Saldarriaga. 2021. "Predicting Non-deposition Sediment Transport in Sewer Pipes Using Random Forest." *Water Research* 189: 116639. doi:10.1016/j.watres.2020.116639.

NEIWPCC. 2003. *Optimizing Operation, Maintenance, and Rehabilitation of Sanitary Sewer Collection Systems*. Lowell, MA: New England Interstate Water Pollution Control Commission.

Ristenpart, E. 1998. "Solids Transport by Flushing of Combined Sewers." *Water Science and Technology* 37 (1): 171–178. doi:10.1016/S0273-1223(97)00767-1.

Rodríguez, J., N. McIntyre, M. Díaz-Granados, and Č. Maksimović. 2012. "A Database and Model to Support Proactive Management of Sediment-related Sewer Blockages." *Water Research* 46 (15): 4571–4586. doi:10.1016/j.watres.2012.06.037.

Saegrov, S. 2006. *Computer Aided Rehabilitation of Sewer and Storm Water Networks – CARE-S*. IWA Publishing. doi:10.2166/9781780402390.

Safari, M. 2020. "Hybridization of Multivariate Adaptive Regression Splines and Random Forest Models with an Empirical Equation for Sediment Deposition Prediction in Open Channel Flow." *Journal of Hydrology* 590: 125392. doi:10.1016/j.jhydrol.2020.125392.

Safari, M., M. Mohammadi, and A. Ab Ghani. 2018. "Experimental Studies of Self-cleansing Drainage System Design: A Review." *Journal of Pipeline Systems Engineering and Practice* 9 (4): 04018017. doi:10.1061/(ASCE)PS.1949-1204.0000335.

Sakakibara, T. 1996. "Sediments Flushing Experiment in a Trunk Sewer." *Water Science and Technology* 33 (9): 229–235. doi:10.1016/0273-1223(96)00391-5.

Saul, A., P. Skipworth, S. Tait, and P. Rushforth. 2003. "Movement of Total Suspended Solids in Combined Sewers." *Journal of Hydraulic Engineering* 129 (4): 298–307. doi:10.1061/(ASCE)0733-9429(2003)129:4(298).

Schaffner, J., and J. Steinhardt 2006. "Numerical Investigation of the Self-acting Flushing System HydroFlush GS in Frankenberg/Germany." Paper presented at the 2th Conference on Sewer Operation and Maintenance, Vienna, October.

Shahsavari, G., G. Arnaud-Fassetta, and A. Campisano. 2017. "A Field Experiment to Evaluate the Cleaning Performance of Sewer Flushing

on Non-uniform Sediment Deposits." *Water Research* 118: 59–69. doi:10.1016/j.watres.2017.04.026.

Shirazi, R., A. Campisano, C. Modica, and P. Willems. 2014. "Modelling the Erosive Effects of Sewer Flushing Using Different Sediment Transport Formulae." *Water Science and Technology* 69 (6): 1198–1204. doi:10.2166/wst.2013.810.

Wan Mohtar, W., H. Afan, A. El-Shafie, C. Bong, and A. Ab Ghani. 2018. "Influence of Bed Deposit in the Prediction of Incipient Sediment Motion in Sewers Using Artificial Neural Networks." *Urban Water Journal* 15 (4): 296–302. doi:10.1080/1573062X.2018.1455880.

Yang, H., D. Zhu, Y. Zhang, and Y. Zhou. 2019. "Numerical Investigation on Bottom Shear Stress Induced by Flushing Gate for Sewer Cleaning." *Water Science and Technology* 80 (2): 290–299. doi:10.2166/wst.2019.269.

Yu, C., and J. Duan. 2014. "Two-Dimensional Finite Volume Model for Sediment Transport in Unsteady Flow." *World Environmental and Water Resources Congress* 2014: 1432–1441. doi:10.1061/9780784413548.144.